Structure of phosphorylated enzyme I, the phosphoenolpyruvate:sugar phosphotransferase system sugar translocation signal protein

Alexey Teplyakov, Kap Lim, Peng-Peng Zhu, Geeta Kapadia, Celia C. H. Chen, Jennifer Schwartz, Andrew Howard, Prasad T. Reddy, Alan Peterkofsky, and Osnat Herzberg

PNAS published online Oct 19, 2006;
doi:10.1073/pnas.0607587103

Structure of phosphorylated enzyme I, the phosphoenolpyruvate:sugar phosphotransferase system sugar translocation signal protein

Alexey Teplyakov*†, Kap Lim*, Peng-Peng Zhu‡, Geeta Kapadia*, Celia C. H. Chen*, Jennifer Schwartz*, Andrew Howard§, Prasad T. Reddy¶, Alan Peterkofsky‡, and Osnat Herzberg*‖

*Center for Advanced Research in Biotechnology, University of Maryland Biotechnology Institute, 9600 Gudelsky Drive, Rockville, MD 20850; ‡Laboratory of Cell Biology, National Heart, Lung, and Blood Institute, National Institutes of Health, Bethesda, MD 20892; §Biological, Chemical, and Physical Sciences, Illinois Institute of Technology, Chicago, IL 60616; and ¶Biochemical Science Division, Chemical Sciences and Technology Laboratory, National Institute of Standards and Technology, Gaithersburg, MD 20899-0001

Communicated by Ada Yonath, Weizmann Institute of Science, Rehovot, Israel, September 7, 2006 (received for review July 24, 2006)

Bacterial transport of many sugars, coupled to their phosphorylation, is carried out by the phosphoenolpyruvate (PEP):sugar phosphotransferase system and involves five phosphoryl group transfer reactions. Sugar translocation initiates with the Mg^{2+}-dependent phosphorylation of enzyme I (EI) by PEP. Crystals of *Escherichia coli* EI were obtained by mixing the protein with Mg^{2+} and PEP, followed by oxalate, an EI inhibitor. The crystal structure reveals a dimeric protein where each subunit comprises three domains: a domain that binds the partner PEP:sugar phosphotransferase system protein, HPr; a domain that carries the phosphorylated histidine residue, His-189; and a PEP-binding domain. The PEP-binding site is occupied by Mg^{2+} and oxalate, and the phosphorylated His-189 is in-line for phosphotransfer to/from the ligand. Thus, the structure represents an enzyme intermediate just after phosphotransfer from PEP and before a conformational transition that brings His-189~P in proximity to the phosphoryl group acceptor, His-15 of HPr. A model of this conformational transition is proposed whereby swiveling around an α-helical linker disengages the His domain from the PEP-binding domain. Assuming that HPr binds to the HPr-binding domain as observed by NMR spectroscopy of an EI fragment, a rotation around two linker segments orients the His domain relative to the HPr-binding domain so that His-189~P and His-15 are appropriately stationed for an in-line phosphotransfer reaction.

sugar transport | phosphorylation | x-ray crystallography

The phosphoenolpyruvate (PEP):sugar phosphotransferase system (PTS) (1) catalyzes the synchronized uptake and phosphorylation of a number of carbohydrates in eubacteria (group translocation) (2, 3). With some variations, the PTS comprises three proteins. In the cytoplasm, PEP phosphorylates enzyme I (EI), which then transfers the phosphoryl group to the histidine phosphocarrier protein, HPr. From HPr, the phosphoryl group is transferred to various sugar-specific membrane associated transporters [enzyme II (EII)], each comprising two cytoplasmic domains, EIIA and EIIB, and an integral membrane domain EIIC. Within EII, EIIA accepts the phosphoryl group from HPr and donates it to EIIB, whereupon EIIC mediates sugar translocation. In addition to controlling sugar translocation, the phosphorylation state of PTS proteins is associated with regulation of metabolic pathways and signaling in bacterial cells (4–8).

The ≈64-kDa EI is a homodimer, which is more tightly associated at the phosphorylated state than the unphosphorylated state (9–14). The phosphorylation by PEP requires Mg^{2+} and targets the Nε atom of His-189 (numbering scheme of EI from *Escherichia coli*) (15). The dimer association rate constant is two to three orders of magnitude slower than typical rates measured for other dimeric proteins, suggesting that oligomerization is accompanied by major conformational rearrangements (13, 16, 17). The monomer–dimer equilibrium has been studied *in vitro* by various methods (18–21), and it has been proposed that the transition plays a regulatory role in the PEP:sugar phosphotransferase system. Yet, transient kinetic studies indicated that the EI dimer phosphorylates HPr without dissociating into monomers (17).

Proteolytic cleavage of EI produces two domains (22, 23). The EI N-terminal domain (EIN, residues 1–230) contains the residue that transfers the phosphoryl group, His-189 (15, 24) and the HPr-binding domain, whereas the EI C-terminal domain (EIC, residues 261–575) binds PEP in the presence of Mg^{2+} (the PEP-binding domain) (22, 25) and mediates dimerization (26, 27). Site-directed mutagenesis showed that Cys-502, located on EIC, is essential for phosphorylation of His-189 by PEP (28). The structure of EIN from *E. coli* has been determined by x-ray crystallography (29) and NMR spectroscopy (30). Its mode of interaction with HPr was characterized by site-directed mutagenesis (27) and NMR spectroscopy (31). An α-helical domain binds HPr (the HPr-binding domain), and an α/β domain bears the phosphorylation active center (the His domain). The His domain is functionally and structurally similar to the phosphohistidine swiveling domain of pyruvate phosphate dikinase (PPDK) (32).

The crystal structure of EIC from *Thermoanaerobacter tengcongensis* has recently been determined (33). *E. coli* and *T. tengcongensis* EIs share 54% amino acid sequence identity, thus the fold of the two proteins is expected to be the same. EIC is a dimer exhibiting the $(\alpha/\beta)_8$ barrel fold. The structural and functional PPDK counterpart of EIC binds PEP and mediates dimerization as well. The EI Cys-502 counterparts in PPDK (and pyruvate kinase) were proposed to play a role in protonation of the PEP pyruvyl moiety after cleavage of the phosphoryl group (32).

Both EI and PPDK must shuttle a phosphoryl group between two destinations. Therefore, the swiveling mechanism of the His domain proposed for PPDK is also likely to be applicable to EI. Here, we describe the 2.7-Å resolution crystal structure of a phosphorylated EI from *E. coli* in complex with Mg^{2+} and

Author contributions: O.H. designed research; A.T., K.L., P.-P.Z., G.K., C.C.H.C., J.S., A.H., P.T.R., A.P., and O.H. performed research; A.T., K.L., and O.H. analyzed data; and A.T., K.L., and O.H. wrote the paper.

The authors declare no conflict of interest.

Freely available online through the PNAS open access option.

Abbreviations: EI, enzyme I; EIN, EI N-terminal domain; EIC, EI C-terminal domain; EII, enzyme II; PEP, phosphoenolpyruvate; PPDK, pyruvate phosphate dikinase; SeMet, selenomethionine.

Data deposition: The atomic coordinates and structure factors have been deposited in the Protein Data Bank, www.pdb.org (PDB ID code 2HWG).

†Present address: Centocor R&D, 145 King of Prussia Road, Radnor, PA 19087.

‖To whom correspondence should be addressed. E-mail: osnat@carb.nist.gov.

Table 1. X-ray data processing and refinement statistics

Data collection	WT EI	SeMet EI
Space group	$P\,2_12_12_1$	$P\,2_12_12_1$
Cell dimensions Å	86.5, 95.2, 167.1	85.5, 94.1, 161.0
Wavelength, Å	1.5418	0.9793
Resolution range, Å	30-2.8 (2.9-2.8)*	50-2.7 (2.8-2.7)*
No. of unique reflections	22,757	36,262
Completeness, %	67.2 (32.4)*	99.5 (98.7)*
Redundancy	2.5	5.8
R_{merge}†	0.140 (0.414)*	0.096 (0.326)*
$\langle I/\sigma(I)\rangle$	6.9 (1.2)*	6.4 (2.8)*
Refinement		
R_{work}†	0.198	0.204
R_{free}†	0.297	0.284
rmsd from ideal geometry		
Bond length, Å	0.011	0.018
Bond angle, °	1.45	1.8

*Statistics for the highest-resolution shell are provided in parentheses.
†$R_{merge} = \Sigma_{hkl}\,[(\Sigma_j|I_j - \langle I\rangle|)/\Sigma_j|I_j|]$; $R_{work} = \Sigma_{hkl}\,||F_o| - |F_c||/\Sigma_{hkl}|F_o|$, where F_o and F_c are the observed and calculated structure factors, respectively. R_{free} is computed for randomly selected reflections omitted from the refinement (3% for WT EI and 5% for SeMet EI).

oxalate. The enzyme adopts a conformation that mimics an intermediate after autophosphorylation, before phosphoryl group transfer to HPr. The structure is consistent with a model that the enzyme uses a swiveling mechanism to deliver the phosphoryl group to HPr.

Results and Discussion

EI Crystallization. An inherent flexibility of EI is required for the His domain to communicate between remote active sites; crystallization of *E. coli* EI required a restriction of this conformational flexibility. The phospho-enzyme was produced by a short-term reaction of EI with Mg^{2+} and PEP. Next, oxalate, a pyruvate enolate mimic known to inhibit PEP-using enzymes (34), was added. Oxalate inhibits phosphorylated EI with a K_i of 0.28 mM (28), an ≈10 times higher affinity for the enzyme than that of pyruvate (2 mM) (35). The analogue of the phosphoenzyme/pyruvyl enolate intermediate fixed the position of the His domain with respect to the PEP-binding domain. Crystals that diffracted x-rays were obtained, albeit highly fragile and easily degraded. The structures of the native and selenomethionine (SeMet)-containing protein were eventually determined by molecular replacement.

Quality of the Model. Because of radiation damage, diffraction data of WT EI, collected at room temperature, were incomplete. The electron density map enabled the building of the His- and the PEP-binding domains, but not the HPr-binding domain. In contrast, the diffraction data from a crystal of the SeMet-containing protein collected at 100 K were complete, revealing the entire molecule. The mean crystallographic temperature factor of the HPr-binding domain (55 $Å^2$) is substantially higher than that of the His domain (32 $Å^2$) and the PEP-binding domain (22 $Å^2$). The two visible domains of WT EI adopt the same structure as those of the SeMet-containing protein. Hence, the following discussion refers to the SeMet-containing protein structure refined at 2.7-Å resolution (Table 1).

The crystal asymmetric unit contains the entire dimer of EI. Each monomer includes residues 2–573, an oxalate molecule, and a magnesium ion. In addition, 214 water molecules were identified. In each monomer, the HPr-binding domain is oriented slightly differently relative to the remaining two domains. Domain motion analysis using the program DynDom (36) shows that the HPr-binding domain in one monomer is rotated by 5° and translated by 1.2 Å compared with the second monomer. Only one residue, Ala-359, exhibits sterically strained backbone conformation (φ = 60°, ψ = −113°). Arg-358 is a residue involved in intricate electrostatic interactions within the PEP-binding site. Both residues are conserved in EI from *T. tengcongensis*, where Ala-359 is also sterically strained. Ala-359 is buried in the core and plays a role in anchoring Arg-358. Sterically strained conformations have been shown to be associated with active sites (37), and EI provides another example of such strain.

Overall Structure. EI phosphorylation followed by addition of oxalate yielded crystals in which Mg^{2+}-oxalate occupies the PEP-binding site in close proximity to His-189∼P, and the His domain interacts closely with the PEP-binding domain. Each of the dimer's protomers contains three domains (Fig. 1*A*); the HPr-binding domain (residues 31–143) and the His domain (residues 1–20 and 149–230) are included within the EIN fragment, and the PEP-binding domain (residues 261–573) corresponds to EIC. The EIN domains exhibit the same folds as those seen first in the crystal structure of the EIN fragment (29), and subsequently in the EIN NMR structure (30). In the HPr-binding domain that forms a four-helix bundle, one of the helices (residues 66–96) has a kink at residue 82, which as the NMR structure of EIN/HPr complex shows (29), provides a pocket for HPr binding. The phosphorylated His-189 resides on the N terminus of one of the helices of the His domain, the domain that exhibits an α/β fold unique to EI and PPDK (32). The polypeptide chain crosses over twice from the His domain to the HPr-binding domain such that the HPr-binding domain is inserted between two β-strands of the His domain.

Two linkers between the HPr-binding and His domains encompassing residues 21–30 and 144–148 run antiparallel to one another in extended conformation different from that seen in the structure of the EIN fragment (29). Consequently, the two domains are oriented differently in the two structures (Fig. 2). In the structure of isolated EIN, one face of the HPr-binding domain contacts the helical side of the His domain, whereas the other face is exposed to solvent. The domain interface is not extensive, though, and involves primarily residues at the tip of the first helical hairpin. The same domain orientation was observed in the complex between EIN with HPr determined by NMR (Fig. 2*A*) (31). In contrast, in the structure presented here, the HPr-binding and His domains are not in contact. As can be seen from the superposition of the EI and EIN structures, the domains move as rigid bodies (Fig. 2*B*). Moreover, assuming that HPr binds to the same region of the HPr-binding domain as determined by NMR spectroscopy, the His domain and HPr are stationed far apart from one another (Fig. 2*C*). Analysis of the quasi-rigid body motion using DynDom (36) shows that the transformation between the extended and more compact conformations involves a 64° rotation around an effective hinge axis running between residues located on the two linkers (22–24 and 145–152) and a 1-Å translation along this axis.

The PEP-binding domain (EIC) forms an $(\alpha/\beta)_8$ barrel with a pair of additional helices at the C terminus. The connecting loops on the C-terminal side of the β-strands form the PEP-binding site. The loops following strands two, three, and six are particularly long and include additional short α-helices. Loops three and six are involved in intersubunit and intrasubunit interactions. The atomic coordinates superimpose well on those of the stand-alone *T. tengcongensis* EIC (33), with a rmsd between 298 common Cα atoms of 1.1 Å. The largest differences occur in loops three and six that shift up to 5 Å. These loops interact with the His domain in the intact *E. coli* EI, and the absence of that domain in the *T. tengcongensis* EIC structure accounts for the differences.

The folds of both the His domain and the PEP-binding domain are similar to those of their PPDK counterparts (32). The His domains can be superimposed with an rmsd value of 1.5 Å for

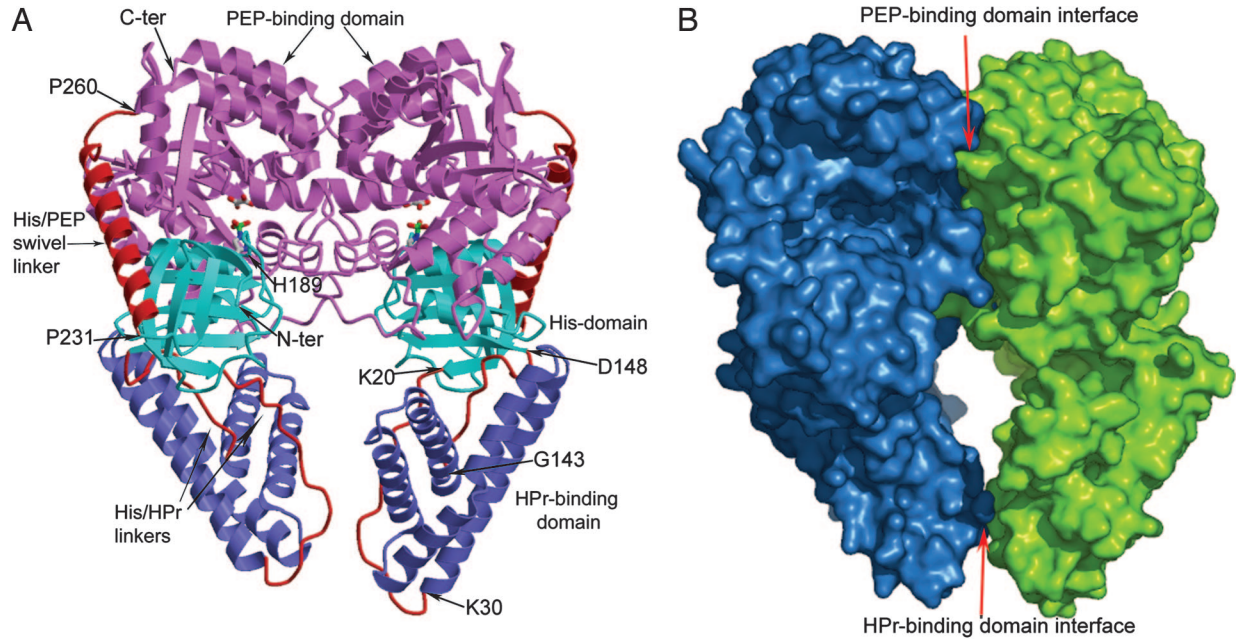

Fig. 1. EI structure. (*A*) Ribbon representation of the dimer. Three linker regions, one between the His and PEP-binding domains and two between the His and HPr-binding domains are highlighted in red. Phosphorylated His-189 and the oxalate are shown as stick models with atomic colors: carbon, gray; oxygen, red; nitrogen, blue; phosphorous, green. (*B*) Surface representation of the dimer in the same orientation as shown in *A*. Each subunit is colored differently.

83 common Cα atoms sharing 28% sequence identity, and superposition of the PEP-binding domains yields an rmsd value of 1.8 Å for 256 Cα atoms sharing 30% sequence identity. Active-site residues show the highest sequence identity and structural similarity.

A 30-residue α-helical linker (residues 231–260) connects the His and PEP-binding domains (Fig. 1). Packing of the helix against the rest of the structure is loose, suggesting potential flexibility that may promote large-scale rearrangement of the domains in the course of the phosphotransfer reaction pathway. Despite the similar fold of both the His and the PEP-binding domains to their PPDK counterparts, the interdomain linker in each enzyme adopts a different conformation. Nevertheless, the presence of flexible linkers supports the notion that both enzymes use the swiveling mechanism to communicate between remote active centers.

Dimer Association. Consistent with mutagenesis studies (26, 27), dimer contacts are mediated by the PEP-binding domain, which is the same not only in intact *E. coli* EI and the stand-alone *T. tengcongensis* EIC (33) but also in three known PPDK structures (32, 38, 39). The angle between a pair of α/β-barrel axes is 67° (axes defined at the center of barrels along the β-strands direction) and the interface is formed at the side of the barrels (Fig. 1). The two PEP-binding sites are located 25 Å apart. Kinetic studies provide no indication of cooperativity between

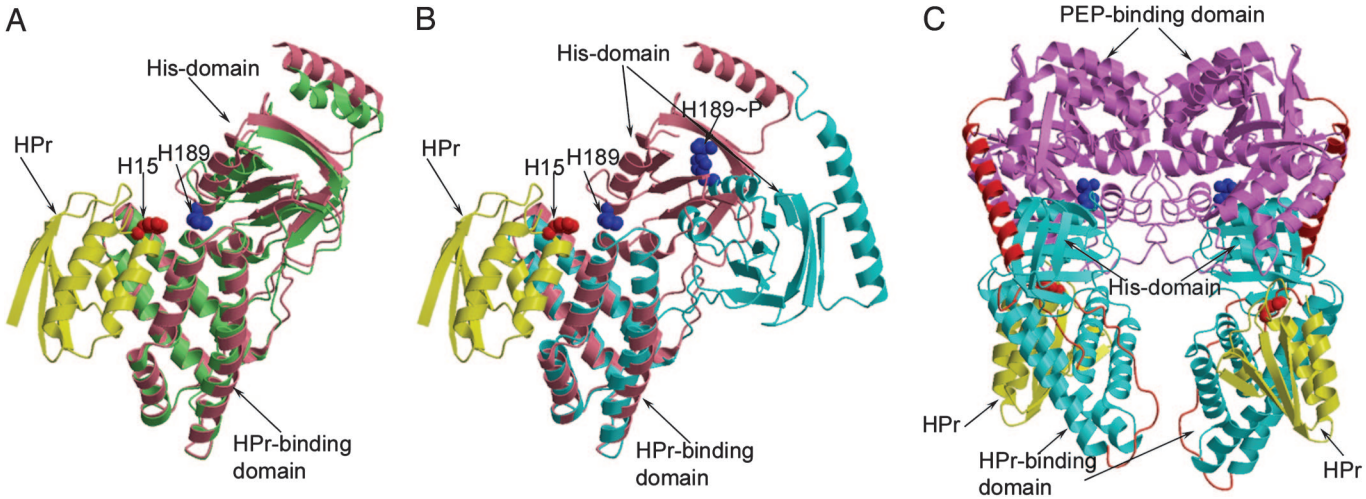

Fig. 2. Superposition of EIN domains. His-189 of EI and His-15 of HPr are shown as space-filling models and are colored blue and red, respectively. (*A*) The crystal structure of the EIN fragment (green) (29) and the NMR structure of the EIN fragment (salmon) in complex with HPr (yellow) (31). (*B*) EIN as determined within the intact EI structure (cyan) together with the NMR structure of the EIN fragment (salmon) in complex with HPr (yellow). (*C*) EI dimer (the PEP-binding domain is colored magenta as in Fig. 1 *A*, EIN is colored cyan as in *B*, and linker regions are colored red) with HPr (yellow) mapped in the same region as in the NMR structure of the EIN/HPr complex.

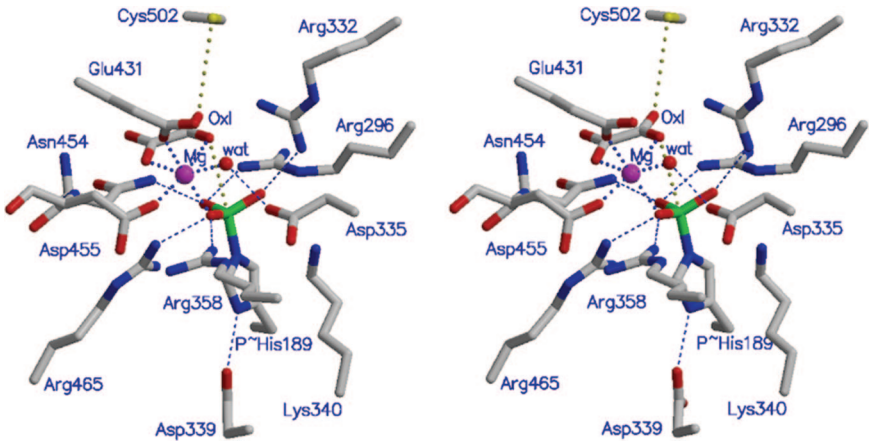

Fig. 3. Stereoscopic representation of key residues in the PEP-binding site. Atomic colors are as defined in Fig. 1. Mg^{2+} is depicted by the magenta sphere. Mg^{2+}–ligand interactions are shown as blue dotted lines, and other electrostatic interactions are shown as blue dashed lines. Cys-502–oxalate and His-189~P–oxalate interactions are shown as yellow dotted lines.

the two subunits (17). The subunit interface is extensive (Fig. 1*B*) and covers 1,800 Å^2 surface area per monomer. The interactions are both hydrophobic and polar and involve residues on loops three and six (residues 338–366 and 453–477), loops that also bear residues that bind the phosphoryl group (Arg-465, Asn-454, and Asp-339, see below). The short α-helix within loop six, spanning residues 453–461 also links activity and dimerization. The C-terminal end of the helix contributes to the dimer interface, whereas the substrate binds at the helix N-terminal end. These key contacts explain the tighter dimer association of phosphorylated EI compared with unphosphorylated EI, and perhaps account for the inactivity of mutant EIs that fail to dimerize (27).

The HPr-binding domain is not involved in oligomerization. Only a few van der Waals contacts occur at the tip of each of the His domains (bottom of Fig. 1*B*), which is enriched with positively charged residues (Arg-28, Lys-29, Lys-30, and Lys-96). The charge clusters on each subunit are related by imperfect symmetry because the like-charges repulse one another, which might have led to the asymmetric disposition of the two HPr-binding domains.

A Snapshot of Phosphotransfer Conformational State. The EI structure corresponds to a conformational state that is relevant not only to EI but also to PPDK function. The PEP-binding site is located at the C-terminal side of the β-barrel, a feature shared with other α/β barrels (40). His-189, on the His domain, is phosphorylated on the Nε atom and projects into the PEP-binding site of the same protomer (Fig. 3), consistent with complementation analysis of EI mutants showing that the phosphoryl group is transferred from PEP to His-189 within a single protein subunit (14, 28). The same arrangement is observed in each of the dimer subunits: The active site is occupied by an octahedrally coordinated Mg^{2+} ion and the inhibitor oxalate. The crystallographic temperature factors of the Mg^{2+}, oxalate, and the phosphoryl group vary between 16 and 25 Å^2, consistent with the crystallographic temperature factors of the surrounding protein residues. Note that pyruvate and oxalate cannot be distinguished at the resolution of the structure determination. However, oxalate is the likely ligand because its K_i (28) is 10-fold lower than the pyruvate's K_m value (35). The failure of EI to crystallize in the absence of oxalate provides further support to the assignment of oxalate as the bound ligand.

Mg^{2+} coordinates two oxygen atoms on the edge of the oxalate molecule [one bonded to the oxalate C(1) and the other to C(2)], and an oxygen atom of the His-189 phosphoryl group (Fig. 3). The carboxylate groups of Glu-431 and Asp-455 and a water molecule that is hydrogen bonded to Asp-335 and Glu-431 complete the octahedral coordination. The observation that Mg^{2+} mediates oxalate (and by analogy PEP) binding is consistent with the report that metal binding precedes substrate binding (41). The catalytic Cys-502 is located within 3.5 Å (average for the two molecules in the asymmetric unit) of the C(2) oxygen atom (Fig. 3), a position that would be occupied by C(3) of pyruvate, which is consistent with the thiol group protonating the pyruvyl enolate from the 2-*re*-face (28). The Nε-P bond of His-189~P is colinear with the oxalate oxygen atom equivalent to the pyruvyl C(2) oxygen atom. Thus, EI has been trapped in a state that mimics an intermediate postphosphorylation but before the His domain undergoing the conformational transition that enables phosphotransfer to HPr. The surface buried upon interaction between the His and the PEP-binding domains is $<$500 Å^2; nevertheless, the convex surface of the His domain complements the concave surface at the center of the PEP-binding domain's α/β barrel and the substrate is shielded from bulk solvent. The only water molecule in the vicinity of the reaction center (3.7 Å away from phosphorous) is the one coordinated by Mg^{2+}; however, it is positioned inappropriately for attack on the phosphoryl group. Hence, desolvation of the active site prevents fortuitous hydrolysis during the phosphotransfer reaction.

Exquisite electrostatic interactions govern the binding site (Fig. 3). Most strikingly, four arginine side chains interact with the phosphoryl group: Arg-296, Arg-332, Arg-358, and Arg-465. In turn, Arg-332 interacts with a oxalate C(2) oxygen, Arg-358 interacts with Asp-455 and Asp-335, and Arg-465 interacts with Asp-455. The oxalate C(1) carboxylate is located in an oxyanion hole formed by the backbone amide group of Asn-454 (whose side chain interacts with the phosphoryl group) and Asp-455 (a Mg^{2+} ligand), both on the N terminus of a two-turn helix (part of loop six). Asp-339 interacts with both the imidazole Nδ atom and the backbone amide of His-189, thus orienting the histidine for in-line phosphotransfer from the PEP to the His domain and enhancing the nucleophilic character of the Nε atom.

Relationship to PPDK. EI Mg^{2+} coordination and electrostatic interactions are similar to those observed in the crystal structures of PPDKs from *Clostridium symbiosum* and maize, the first structure determined in complex with Mg^{2+}-phosphonopyruvate, and the second in complex with Mg^{2+}-PEP (39, 42). The catalytic mechanism involving protonation of the pyruvyl enolate product by a cysteine residue is conserved in PPDK, with the Cys-831 (numbering scheme based on the enzyme from *C. symbiosum*) stationed appropriately for the acid/base catalysis. Thus, EI and PPDK use the same substrate-binding mode, in agreement with early studies that implied that the two enzymatic reactions follow an in-line phosphotransfer mechanism involving pentacoordinated phosphorous with trigonal bipyramidal geometry, and the donor (PEP) and acceptor (His-189 in EI, His-455 in PPDK) in the apical positions (43–45).

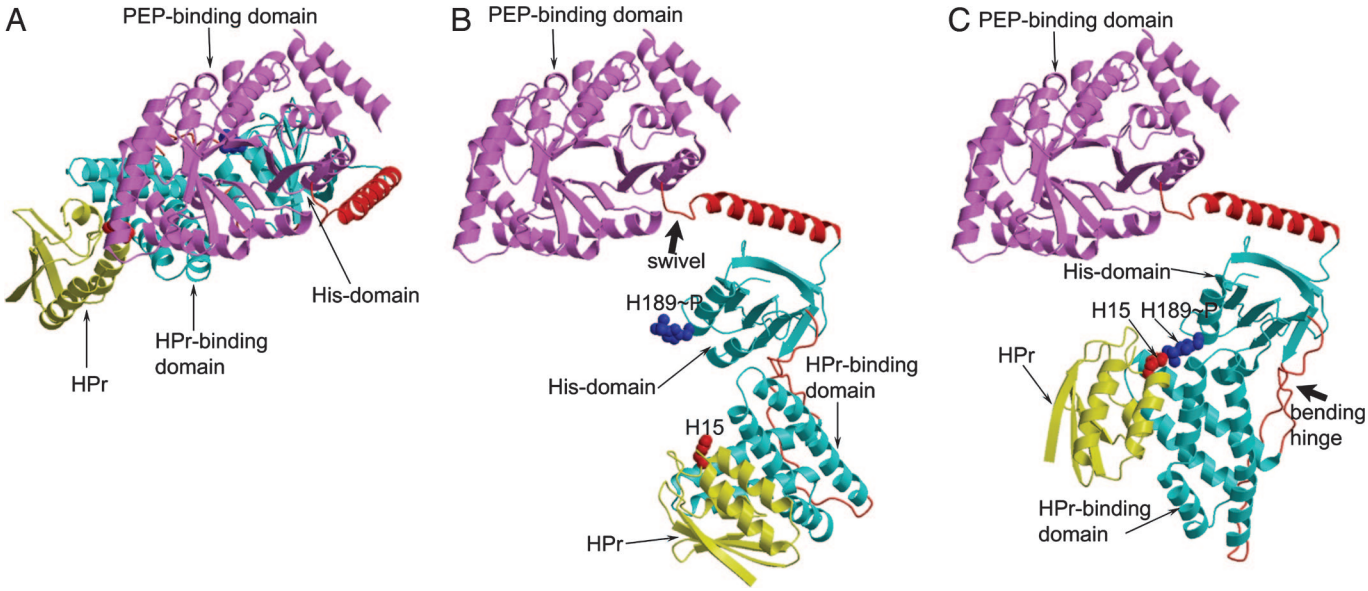

Fig. 4. Proposed EI flexibility loci used in phosphotransfer to HPr. Three conformational states are shown, using the same orientation of the PEP-binding domain as a reference to illustrate the extent of motion. Domain colors are as in Fig. 2*C*. His-189~P of EI and His-15 of HPr are shown as space-filling models and are colored blue and red, respectively. (*A*) Subunit conformation as in the current EI structure. HPr (yellow) is placed to interact with the same region as in the NMR structure of the EIN/HPr complex (31). (*B*) The swivel around the helical linker. His-189 of EI and His-15 are too far apart for phosphotransfer to occur. (*C*) Following step B, the His domain of the EIN/HPr NMR structure was superposed on the EI His domain, and the relative orientations of the HPr-binding domain and HPr were transformed to the EI model (i.e., the two EI moving domains and HPr are the same as in the NMR structure). The effective hinge axis that corresponds to this transformation runs between residues 22–24 and 145–152. His-189 of EI and His-15 of HPr are now in line for phosphotransfer to take place. The conformation of His-189 is as in the EI crystal structure, which is different from that seen in the EIN crystal and NMR structures.

Many residues surrounding the PEP binding site are conserved in EI and PPDK. Most notably, the EI guanidinium groups that interact with the phosphoryl group (Arg-296, Arg-332, Arg-358, and Arg-465) have counterparts in PPDK (Arg-561, Arg-617, Arg-665, and Arg-779, respectively). Site-directed mutagenesis of Arg-561 and Arg-617 in PPDK resulted in inactivation of the enzyme, even for the conservative replacement to a lysine (42). The residues forming an oxyanion hole that accommodates the carboxylate group of PEP/pyruvate are also conserved; Asn-768 and Asp-767 in PPDK are analogous to Asn-454 and Asp-455 in EI. Finally, the PPDK counterpart of EI's Asp-339 may be Glu-625. Both residues are located on loop three, which vary in length and conformation in the two enzymes. Because of the different loop three, it remains to be seen whether Glu-625 plays the same role as Asp-339 of EI. Based on the currently available PPDK structures, this would necessitate that loop three changes conformation.

The Swiveling Mechanism of EI. The NMR structure of EIN in complex with HPr revealed that the EIN-HPr interface is centered on a EI region enriched with hydrophobic residues (Ala-71, Ile-72, Gly-75, Met-78, Leu-79, Leu-115, and Leu-126) (31). A cluster of EI interhelical residues (Leu-79, Leu-85, Val-30, and Leu-133) form a pocket that accommodates Phe-48 of HPr, providing interaction specificity. The EI positively charged invariant residues, Arg-126 and Lys-69 (together with Arg-17 on HPr), are in position to stabilize phosphotransfer. In the crystal structure of the intact phosphorylated EI, this surface is remote from the PEP binding site (≈40 Å separation, Fig. 2*C*). Clearly, when buried in the PEP-binding site, His-189~P cannot interact with His-15 of HPr. Moreover, the position of the His domain is near the face of the HPr-binding domain opposite to that shown to participate in the EI-HPr interface (Figs. 2*C* and 4*B*). Therefore, the His domain must undergo a large conformational change to disengage from the PEP-binding domain and be placed in proximity to HPr, with His-189~P appropriately oriented for in-line phosphotransfer to the His-15 Nδ atom of HPr.

A model of the productive complex between EI~P and HPr was generated by rotating domains as rigid bodies around two axes (Fig. 4). The first rotation swivels the helical linker (residues 231–260) together with the His and HPr-binding domains away from the PEP-binding domain. A wide range of rotation angles is possible, giving rise to different relative orientation of EIN and EIC. The model shown in Fig. 4*B* depicts one possibility, which corresponds to 95° rotation generated by modifying the backbone dihedral angles of Leu-259 and Pro-260, linker residues that follow the C terminus of the helix. This motion does not affect the His-189–His-15 distance (≈30 Å). To bring His-189~P in proximity to His-15 of HPr, assuming the same interface as that determined by NMR spectroscopy, the orientation of the HPr-binding domain relative to the His domain has to be modified as shown in Fig. 2*C*. The rigid body transformation of the HPr-binding domain consists of 64° rotation along the hinge axis running between residues 22–24 and 145–152, which results in the structure depicted in Fig. 4*C*. His-189~P and His-15 of HPr are now close together.

As it appears in the various structures of the EIN fragment, either EIN alone or in complex with HPr, the Nε atom of His-189 is buried and interacts with the hydroxyl group of Thr-168. Such side-chain conformation is incompatible with phosphorylation and phosphotransfer. In contrast, the conformation of His-189~P is appropriate for phosphoryl group transfer vis-à-vis its interaction with oxalate, thus the same side-chain conformation is also compatible with phosphotransfer to His-15 of HPr. The adjustment of His-189~P side-chain conformation allows phosphotransfer that follows the associative mechanism (43), as can be seen in Fig. 4*C*. The multiple positively charged residues that surround the phosphohistidine residue (Arg-126 and Lys-69 on EI; Arg-17 on HPr) are analogous to the multiple positively charged residues within the PEP-binding domain that stabilize the phosphoryl group. Finally, unlike the complementary sur-

faces of the His and PEP-binding domain interface, the His domain and HPr do not interact with one another. Instead, the precise positioning of HPr is accomplished by complementing a HPr-binding domain surface.

In summary, the model demonstrates that the conformational transitions associated with phosphotransfer to HPr involve rigid body domain motions, which is achievable without major steric clashes and while maintaining the dimeric association of EI. From a structural point of view, phosphotransfer from the His domain to HPr needs not be carried out synchronously by the two subunits. We emphasize that the model is not necessarily accurate in details; the swivel angle may vary, and some backbone and side chains may undergo structural adjustments concomitant with the changes in linker conformations. The crystal structure and the proposed conformational transition are consistent with the associative pathway and in-line phosphoryl group transfer.

While this article was being reviewed, the crystal structure of apo-EI from *Staphylococcus carnosus* was published (46). The His domain in this structure is largely disordered; however, the helical linker is defined and confirms our swiveling domain hypothesis.

Materials and Methods

Protein was expressed and purified as described (47). Crystals of the WT enzyme were obtained at room temperature by vapor diffusion in hanging drops. The protein sample (10 mg/ml) was mixed with $MgCl_2$ and PEP to a final concentration of additives of 10 mM. After ≈5 min, sodium oxalate was added to a final concentration of 10 mM. Drops containing 1:1 protein and reservoir solution were equilibrated against reservoir solution containing 22% (wt/vol) polyethylene glycol 6000, 2% saturated ammonium sulfate, and 100 mM Na^+·Hepes (pH 7.0). The procedure for crystallization of the SeMet-containing protein was the same as above except that the reservoir solution contained 24% (wt/vol) polyethylene glycol monomethyl ether 2000, 4% saturated ammonium sulfate, 0.5 mM oxalate, and 100 mM Na^+·Hepes (pH 7.0). X-ray diffraction data for the WT protein crystal were collected at room temperature on a Rigaku (Tokyo, Japan) Rotaflex RU200BH rotating anode equipped with a Siemens (Iselin, NJ) area detector, and those for the SeMet-containing protein crystal were collected at 100 K on the IMCA-CAT 17-ID beamline at the Advanced Photon Source (Argonne National Laboratory, Argonne, IL) equipped with a MAR CCD (Norderstedt, Germany) detector. The structures were determined by molecular replacement using the program PHASER (48) and the structure of EIC from *T. tengcongensis* (33) as an initial search model. Refinement was carried out with the programs REFMAC (49) and CNS (50). A detailed description of the methods is available in *Supporting Text*, which is published as supporting information on the PNAS web site, and an electron density map in the region of the PEP binding site is shown in Fig. 5, which is published as supporting information on the PNAS web site.

The work was supported by National Science Foundation Grant MCB9813271 (to O.H.). Use of the Advanced Photon Source was supported by the U.S. Department of Energy, Basic Energy Sciences, Office of Science, under Contract W-31-109-Eng-38.

1. Kundig W, Ghosh S, Roseman S (1964) *Proc Natl Acad Sci USA* 52:1067–1074.
2. Meadow ND, Fox DK, Roseman S (1990) *Annu Rev Biochem* 59:497–542.
3. Postma PW, Lengeler JW, Jacobson GR (1993) *Microbiol Rev* 57:543–594.
4. Commichau FM, Forchhammer K, Stulke J (2006) *Curr Opin Microbiol* 9:167–172.
5. Saier MH, Jr, Reizer J (1994) *Mol Microbiol* 13:755–764.
6. Saier MH, Jr, Chauvaux S, Deutscher J, Reizer J, Ye JJ (1995) *Trends Biochem Sci* 20:267–271.
7. Warner JB, Lolkema JS (2003) *Microbiol Mol Biol Rev* 67:475–490.
8. Stulke J, Hillen W (1998) *Naturwissenschaften* 85:583–592.
9. Waygood EB, Meadow ND, Roseman S (1979) *Anal Biochem* 95:293–304.
10. Saier MH, Jr, Schmidt MR, Lin P (1980) *J Biol Chem* 255:8579–8584.
11. Misset O, Brouwer M, Robillard GT (1980) *Biochemistry* 19:883–890.
12. Kukuruzinska MA, Turner BW, Ackers GK, Roseman S (1984) *J Biol Chem* 259:11679–11681.
13. Chauvin F, Brand L, Roseman S (1996) *Res Microbiol* 147:471–479.
14. Seok YJ, Zhu PP, Koo BM, Peterkofsky A (1998) *Biochem Biophys Res Commun* 250:381–384.
15. Alpert CA, Frank R, Stuber K, Deutscher J, Hengstenberg W (1985) *Biochemistry* 24:959–964.
16. Chauvin F, Brand L, Roseman S (1994) *J Biol Chem* 269:20270–20274.
17. Meadow ND, Mattoo RL, Savtchenko RS, Roseman S (2005) *Biochemistry* 44:12790–12796.
18. Dimitrova MN, Szczepanowski RH, Ruvinov SB, Peterkofsky A, Ginsburg A (2002) *Biochemistry* 41:906–913.
19. Dimitrova MN, Peterkofsky A, Ginsburg A (2003) *Protein Sci* 12:2047–2056.
20. Ginsburg A, Peterkofsky A (2002) *Arch Biochem Biophys* 397:273–278.
21. Patel HV, Vyas KA, Savtchenko R, Roseman S (2006) *J Biol Chem* 281:17570–17578.
22. LiCalsi C, Crocenzi TS, Freire E, Roseman S (1991) *J Biol Chem* 266:19519–19527.
23. Lee BR, Lecchi P, Pannell L, Jaffe H, Peterkofsky A (1994) *Arch Biochem Biophys* 312:121–124.
24. Weigel N, Kukuruzinska MA, Nakazawa A, Waygood EB, Roseman S (1982) *J Biol Chem* 257:14477–14491.
25. Seok YJ, Lee BR, Zhu PP, Peterkofsky A (1996) *Proc Natl Acad Sci USA* 93:347–351.
26. Zhu PP, Szczepanowski RH, Nosworthy NJ, Ginsburg A, Peterkofsky A (1999) *Biochemistry* 38:15470–15479.
27. Brokx SJ, Talbot J, Georges F, Waygood EB (2000) *Biochemistry* 39:3624–3635.
28. Garcia-Alles LF, Alfonso I, Erni B (2003) *Biochemistry* 42:4744–4750.
29. Liao DI, Silverton E, Seok YJ, Lee BR, Peterkofsky A, Davies DR (1996) *Structure (London)* 4:861–872.
30. Garrett DS, Seok YJ, Liao DI, Peterkofsky A, Gronenborn AM, Clore GM (1997) *Biochemistry* 36:2517–2530.
31. Garrett DS, Seok YJ, Peterkofsky A, Gronenborn AM, Clore GM (1999) *Nat Struct Biol* 6:166–173.
32. Herzberg O, Chen CC, Kapadia G, McGuire M, Carroll LJ, Noh SJ, Dunaway-Mariano D (1996) *Proc Natl Acad Sci USA* 93:2652–2657.
33. Oberholzer AE, Bumann M, Schneider P, Bachler C, Siebold C, Baumann U, Erni B (2005) *J Mol Biol* 346:521–532.
34. Seidel HM, Knowles JR (1994) *Biochemistry* 33:5641–5646.
35. Rohwer JM, Meadow ND, Roseman S, Westerhoff HV, Postma PW (2000) *J Biol Chem* 275:34909–34921.
36. Hayward S, Berendsen HJ (1998) *Proteins* 30:144–154.
37. Herzberg O, Moult J (1991) *Proteins* 11:223–229.
38. Cosenza LW, Bringaud F, Baltz T, Vellieux FM (2002) *J Mol Biol* 318:1417–1432.
39. Nakanishi T, Nakatsu T, Matsuoka M, Sakata K, Kato H (2005) *Biochemistry* 44:1136–1144.
40. Brändén C-I (1980) *Q Rev Biophys* 13:317–338.
41. Patel HV, Vyas KA, Mattoo RL, Southworth M, Perler FB, Comb D, Roseman S (2006) *J Biol Chem* 281:17579–17587.
42. Herzberg O, Chen CC, Liu S, Tempczyk A, Howard A, Wei M, Ye D, Dunaway-Mariano D (2002) *Biochemistry* 41:780–787.
43. Knowles JR (1980) *Annu Rev Biochem* 49:877–919.
44. Begley GS, Hansen DE, Jacobson GR, Knowles JR (1982) *Biochemistry* 21:5552–5556.
45. Cook AG, Knowles JR (1985) *Biochemistry* 24:51–58.
46. Marquez JA, Reinelt S, Koch B, Engelmann R, Hengstenberg W, Scheffzek K (2006) *J Biol Chem*, in press.
47. Reddy P, Fredd-Kuldell N, Liberman E, Peterkofsky A (1991) *Protein Expression Purif* 2:179–187.
48. Read RJ (2001) *Acta Crystallogr D* 57:1373–1382.
49. Winn MD, Isupov MN, Murshudov GN (2001) *Acta Crystallogr D* 57:122–133.
50. Brünger AT, Adams PD, Clore GM, DeLano WL, Gros P, Grosse-Kunstleve RW, Jiang JS, Kuszewski J, Nilges M, Pannu NS, *et al.* (1998) *Acta Crystallogr D* 54:905–921.